Measuring microwave properties of laminated dielectric substrates

V. N. Egorov and V. L. Masalov
East-Siberian Research Institute of Physico-Technical and Radioengineering Measurements, 57, Borodina str., Irkutsk, 664056, Russia

Yu. A. Nefyodov,[a] A. F. Shevchun, and M. R. Trunin
Institute of Solid State Physics RAS, Chernogolovka, Moscow district, 142432, Russia

(Received 31 March 2004; accepted 16 July 2004)

The theoretical approach is developed and the test rig is designed for measuring the microwave parameters of dielectric substrates at frequencies between 30 and 40 GHz and over a temperature range from −50 to +70 °C. The test rig is based on sapphire resonators and allows the measurements of the following parameters of commonly used PCB materials: (i) dielectric constant (ε) of the dielectric substrate in the range from 2 to 10, (ii) loss tangent ($\tan\delta$) of the substrate in the range from 10^{-4} to 10^{-2}, and (iii) ranging from 0.03 to 0.3 Ωsurface resistance of the laminating metal layer adjoining the dielectric material. © *2004 American Institute of Physics.*
[DOI: 10.1063/1.1791315]

I. INTRODUCTION

Essential parameters needed for the efficient design of microwave printed circuit boards (PCBs) are dielectric properties (ε and $\tan\delta$) of the substrate on which the active elements are placed and the surface resistance R_S of the PCB lamination metal. As components are increasingly miniaturized and frequencies increase, the need for accurate measurements of low-loss substrate materials increases. The properties of these materials should also be known in a wide temperature range.

Resonant measurement methods represent the most accurate way of obtaining dielectric constant and loss tangent of unclad thin materials.[1] The high value of the unloaded quality factor Q_0 appears to be essential parameter of the resonator. The higher Q_0 the smaller losses in the test materials can be measured. The methods based on bulk resonators have been developed in many laboratories and the results have been widely published.[1–4] The cylindrical H_{01p} cavity has been used to measure both the in-plane dielectric parameters of thin dielectric samples as well as the surface resistance of normal metals and low- and high-temperature superconductors.[5–9] However, at room temperature the Q_0 value of bulk resonators does not exceed 10^4 in the millimeter wavelength band. The open hemispherical resonator,[2,3,10] is a very sensitive instrument for in-plane dielectric measurements of extremely low-loss and flat specimens with diameters much greater than the wavelength. There are two problems within this approach: nonflatness of real samples and large resonator sizes. Microstrip based tests[11] do not allow the dielectric and ohmic losses to be measured separately. The nonreproducibility of the rig connection impedance limits also the accuracy of this method. A cylindrical $H_{01\delta}$ dielectric split resonator[12] made from thermostable high-permittivity ceramics has been successfully used for in-plane dielectric film measurements at frequencies below 10 GHz, but it was found unsuitable for measurements at higher frequencies due to increasing loss tangent of the ceramics used and, hence, decreasing Q_0.

In all the above-mentioned methods microwave E-field is parallel to the specimen interface surface. At the same time, in most PCBs the electric field is primarily orthogonal to the sheet plane. Thus, it will be preferable if the electromagnetic field in the measurement setup has an electric field component orthogonal to the sample surface. The sapphire disk whispering gallery (WG) resonator[13] has Q_0 about 40 000 at room temperature in 40 GHz frequency range (wavelength λ of about 8 mm) and typical diameter about 1.5λ. There are two WG mode types: quasi-E (or HE) and quasi-H (or EH) having high Q_0 value for large azimuth mode index $n \gg 1$. They can be used for dielectric substrate measurements with orthogonal and tangential microwave E-field, respectively. There is a general and significant problem when performing measurements with an orthogonal field, namely, the so-called "residual air-gap" which exists due to micro-roughness at the contact between the flat resonator and the specimen surface. It does affect the measurable quantities and should be accounted for by the electrodynamic model of the measured structure.

The goal of this paper is to evaluate both theoretically and experimentally the pros and cons of the sapphire disk WG resonator (DR) technique for measurements of the out-of-plane dielectric properties of thin materials using up to five different HE_{n11} modes. Reasonable accuracy of the measurements was provided both for extremely thin substrates with a thickness down to 50 μm as well as for very thick substrates with a thickness exceeding 1 mm. This became possible owing to the fact that the DR has high Q_0 value and substantial filling factor even with very thin substrates. An accuracy of 1% for permittivity measurements and a resolution of the order of 10^{-4} for their loss tangent has been shown at 40 GHz. Also our test method allows the measure-

[a]Electronic mail: nefyodov@issp.ac.ru

 © 2004 American Institute of Physics

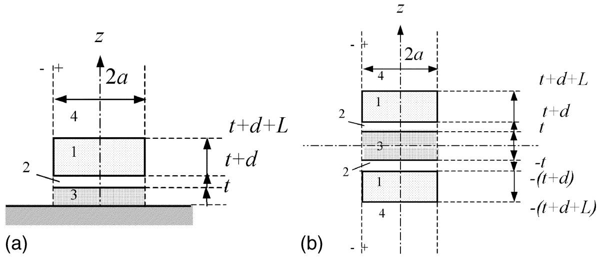

FIG. 1. (a) DR 1 above a metallic plane with dielectric layer 3 inserted in between; the residual air gap 2 is also shown; (b) dielectric layer in the split DR.

ments of the effective microwave surface resistance of the laminating metal at the interface with the dielectric material.

In the next section, we discuss the structure of the electromagnetic field in the DR and the theoretical model used for calculating the microwave parameters for unclad and laminated substrates. In Sec. III, we present the details of the test rig design, the experimental procedures, and raw data processing. In Appendix A we present further details of the distribution of the longitudinal and transverse field components in the DR. Finally, measurements results for a number of commonly-used microwave PCB materials are given in Appendix B in the table form.

II. ELECTRODYNAMICS

A. Measurement structure basis

Below we describe the resonance mode structure of a dielectric cylinder [Fig. 1(a)] having diameter $2a$ and height L, which is separated from a metallic plane by a dielectric layer of height t and a gap of height d. If the component of the electric field in z direction $E_z(z)$ is an even function of z, then the plane $z=0$ (metallic surface) behaves as the so-called "electric wall" for which the following boundary conditions apply: $E_{3r}=E_{3\varphi}=0$. In such a case the electromagnetic field structure is equivalent to the one for the split DR with a dielectric layer of double height $2t$ in the slot [Fig. 1(b)].

The relative permittivity of a DR is characterized by a tensor

$$\hat{\varepsilon}_1=\begin{pmatrix}\varepsilon_{1\perp} & 0 & 0\\ 0 & \varepsilon_{1\perp} & 0\\ 0 & 0 & \varepsilon_{1\|}\end{pmatrix},$$

which determines the electric properties, and by a scalar μ_1 for the magnetic ones. Symbols $\|$ and $\perp$ denote the components of $\hat{\varepsilon}_1$ in the direction along the optical (geometrical) axis and in the plane perpendicular to this axis, respectively. We use ε_3, μ_3 for the isotropic dielectric layer, and ε_2, μ_2 for the ambient isotropic space, which includes both the top space 4 and the gap 2. We analyze the electromagnetic resonance modes by the method of approximate separation of variables with one-mode approximation of the fields at all fractional volumes of the resonator.[5] Within the limits of this approach the electromagnetic field of the frequency ω inside the DR within the boundaries $t+d \leqslant z \leqslant t+d+L$ is represented in the form of linear combination of standing E- and H- waves, which form a hybrid standing HE or EH wave along the z-axis. Transverse (on r, φ coordinates) field distribution in the gap 2, the dielectric layer 3 and the top space 4 is assumed to be the same as in the disk 1. Further details of the derivation of equations for the electromagnetic field components are given in Appendix A. Both the longitudinal wave numbers h_{1E} and h_{1H} of the E- and H-waves, respectively, are equal to the longitudinal wave number of the hybrid wave in the disk 1: $h_{1E}=h_{1H}=h$.

The boundary conditions $E^{+}_{1\varphi}=E^{-}_{1\varphi}, H^{+}_{1\varphi}=H^{-}_{1\varphi}$ for inside (+) and outside (–) field components at $r=a$ within the limits $t+d \leqslant z \leqslant t+d+L$ $(i=1)$ define the equation of a circular "dielectric post resonator" with uniaxial anisotropy:[13]

$$\left[\frac{\varepsilon_{\|}J_n'(\alpha\chi_1 a)}{\alpha\chi_1 a J_n(\alpha\chi_1 a)}-\frac{H_n^{(2)\prime}(\chi_2 a)}{\chi_2 a H_n^{(2)}(\chi_2 a)}\right]\left[\frac{\mu J_n'(\chi_1 a)}{\chi_1 a J_n(\chi_1 a)}-\frac{H_n^{(2)\prime}(\chi_2 a)}{\chi_2 a H_n^{(2)}(\chi_2 a)}\right]-\left(\frac{nh}{k_2}[(\chi_1 a)^{-2}-(\chi_2 a)^{-2}]\right)^2=0, \quad (1)$$

where $J_n(\chi_1 a), H_n^{(2)}(\chi_2 a)$, $J_n'(\chi_1 a), H_n^{(2)\prime}(\chi_2 a)$ are the Bessel and Hankel functions of the order n and their derivatives, χ_1, χ_2 are the inside (+) and outside (-) transverse wave numbers, respectively, and $\varepsilon_{\|}=\varepsilon_{1\|}/\varepsilon_2$, $\mu=\mu_1/\mu_2$, $\alpha=\sqrt{\varepsilon_{1\|}/\varepsilon_{1\perp}}$. For $\varepsilon_{\|}=\varepsilon_{\perp}\equiv\varepsilon_{1\perp}/\varepsilon_2$ this equation is reduced to the equation of an isotropic "dielectric post resonator."

For HE_{nmp} modes with odd longitudinal index $p=2q+1(q=0,1,2,\ldots)$ the boundary conditions at $z=0$, $z=t$, $z=t+d$, $z=t+d+L$ result in the characteristic equation[14]

$$hL-\arctan\frac{h_{2E}\eta_{1E}}{h}-\arctan\left(\frac{h_{2E}\eta_{1E}}{h}\times\tanh\left[\operatorname{arctanh}\left(\frac{h_{3E}}{h_{2E}\eta_{3E}}\tanh(h_{3E}t)\right)+h_{2E}d\right]\right)-(p-1)\pi=0, \quad (2)$$

where h_{iE} are the longitudinal wave numbers in regions $i=2,3,4$ (Fig. 1), $h_{2E}=h_{4E}$

$$h=\sqrt{k_1^2-\chi_1^2}=\sqrt{k_2^2-\chi_2^2}, \quad h_{2E}=\sqrt{(\alpha\chi_1)^2-k_2^2},$$
$$h_{3E}=\sqrt{(\alpha\chi_1)^2-k_3^2},$$
$$k_1=k_0\sqrt{\varepsilon_{1\perp}\mu_1}, \quad k_2=k_0\sqrt{\varepsilon_2\mu_2}, \quad k_3=k_0\sqrt{\varepsilon_3\mu_3},$$
$$k_0=\omega\sqrt{\varepsilon_0\mu_0},$$
$$\eta_{1E}=\varepsilon_{1\perp}/\varepsilon_2, \quad \eta_{3E}=\varepsilon_3/\varepsilon_2.$$

The set of Eqs. (1) and (2) defines the values of h, χ_1 and $k_1=\sqrt{h^2+\chi_1^2}$, which depend on the relative dielectric permittivity of the sample $\varepsilon=\varepsilon_3/\varepsilon_2$. Equation (1) does not explicitly depend on ε and, thus, to determine ε one should solve Eqs. (1) and (2) in series with the values of k_1, k_2 at the measured resonance frequencies.

The schematic fragment of the electromagnetic field structure for HE_{n11} resonant mode is shown in Fig. 2(a). Figure 2(b) demonstrates the $E_z(r,\varphi)$ field relief and its level lines for a particular HE_{911} mode.

The electrodynamic model described by Eqs. (1) and (2) does not allow for an influence of the part of the dielectric sample at $r>a, 0\leqslant|z|\leqslant t$, i.e., outside the resonator. If this sample volume is taken properly into account, the resonant frequencies will decrease and, hence, Eqs. (1) and (2) will

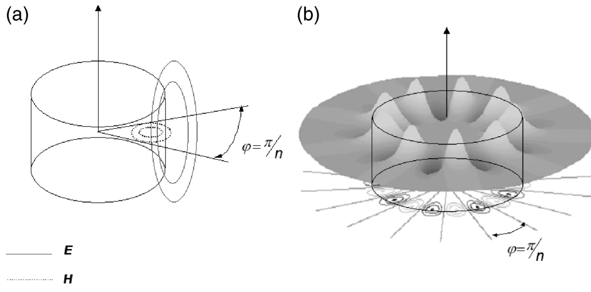

FIG. 2. (a) Schematic fragment of the electromagnetic field structure for HE_{n11} mode; (b) E_z field relief and its level lines for $n=9$.

overestimate the value of ε. Keeping in mind that just a small part of the total electromagnetic energy is stored in the dielectric sample volume outside the resonator, one can correct the value of the dielectric constant by the perturbation method

$$\varepsilon_{\text{corr}} = \varepsilon \cdot [1-(\varepsilon-1)K_{2E}], \tag{3}$$

where $K_{2E}=W_2^E/W_\Sigma=-2(\varepsilon_2/\omega)(\partial\varepsilon_2/\partial\omega)^{-1}$ and W_Σ, W_2^E are the total resonator energy and electric field energy outside the resonator disks. Factor K_{2E} can be found by numerical differentiation of Eqs. (1) and (2) with respect to the ambient media permittivity ε_2 (Ref. 15) and has a typical value of the order of 0.01–0.02. More precisely this value can be obtained by calibrating the test system using a number of dielectric samples with different thickness and known ε.

The frequencies of HE_{nmp} modes in the DR of height L on the metallic plane ($t=0$, $d=0$) coincide with the frequencies of $HE_{nm2\ p-1}$ modes of the DR with height $2L$ in free space. This becomes quite evident from Eq. (2) if one substitutes $L\rightarrow 2L$, $p\rightarrow 2p-1$.

B. Dielectric permittivity and loss tangent measurements of unclad substrates

For the measurements of the dielectric permittivity and loss tangent of the substrate, the foil is removed from both sides of the PCB sample. The sample (substrate) is clamped between the plates of the split DR [Fig. 1(b) and Fig. 6(a) below]. In the experiment the values of the resonant frequencies of HE_{n11} modes are determined. The following data have to be known for calculation of the sample dielectric permittivity using formulas (1) and (2): (i) resonant frequencies f_n of HE_{n11} modes with known azimuth indexes n; (ii) dimensions a,L of the DR; (iii) sapphire dielectric permittivities $\varepsilon_{1\parallel}$,$\varepsilon_{1\perp}$, and (iiii) the thickness t of the sample. The value of the residual air-gap d is determined by the roughness of the surfaces of both the measured sample and the faces of the DR and cannot be measured directly. The frequency dispersion of low-loss dielectric samples in such a narrow frequency range is usually negligible in comparison with the uncertainty of the real measurements. The residual air-gap slightly reduces the measured value ε_3 and makes an additional contribution to inaccuracy. This contribution depends on the frequency and decreases with the increase of the azimuth index n of the resonant mode. Hence, one can estimate d value from the condition that the measured ε_3 value should remain constant at the resonance frequencies of several neighboring $HE_{n-1,1,1}$, $HE_{n,1,1}$, $HE_{n+1,1,1}$ modes.

The electromagnetic power $P_{\delta 3}$ directly absorbed by the sample [dielectric layer 3 in Fig. 1(b)] and electric energy W_3^E stored in the sample layer are connected by the relationship $P_{\delta 3}=\omega W_3^E \tan\delta$, where δ is the dielectric loss angle of the sample. In the usual approximation of the additive contribution of different losses, the power $P_{\delta 3}$ is related to the total power loss P_Σ and the unloaded quality factor $Q_{0\Sigma}$ of the resonator by the following equation:

$$\frac{1}{Q_{0\Sigma}} = \frac{P_\Sigma}{\omega W_\Sigma} = \frac{P_{\delta 1}+P_{\delta 3}+P_{\text{rad}}}{\omega W_\Sigma} = \frac{1}{Q_{0\text{DR}}} + \frac{W_3^E}{W_\Sigma}\tan\delta + \frac{1}{Q_{\text{rad}}}, \tag{4}$$

where $P_{\delta 1}$ is a dielectric loss power in the resonator dielectric disks only; Q_{ODR} is a partial quality factor of these disks; P_{rad} is the radiant loss power; Q_{rad} is the radiant quality factor of the resonator. It is easy to satisfy the condition $Q_{0\text{DR}}^{-1}+W_3^E\tan\delta/W_\Sigma \gg Q_{\text{rad}}^{-1}$ by choosing dimensions of the DR. In this case we get from Eq. (4)

$$\tan\delta = K_{3E}^{-1}(Q_{0\Sigma}^{-1}-Q_{0\text{DR}}^{-1}), \tag{5}$$

where $K_{3E}=W_3^E/W_\Sigma$ is a filling factor of the DR. The value of K_{3E} can be obtained from the value of the stored energy by integrating the field components over the corresponding volumes of the DR

$$W_i^E = \frac{\varepsilon_0\varepsilon_i}{2}\int_{V_i}|\vec{E}|^2 dV, \quad W_\Sigma = \sum_i W_i^E = \sum_i W_i^H, \quad i=1,2,3,4, \tag{6}$$

where $W_i^{E,H}$ is the energy of electric (magnetic) field stored in the V_i-volume of the resonator. Another way to calculate K_{3E} is the numerical differentiation of the $\varepsilon_3(\omega)$ function obtained from Eqs. (1) and (2) at measured resonant frequencies ω of the resonator with the sample inside[15]

$$K_{3E} = -2\frac{\varepsilon_3}{\omega}\left(\frac{\partial\varepsilon_3}{\partial\omega}\right)^{-1}. \tag{7}$$

The quantity $Q_{0\text{DR}}$ in Eq. (5) is the unloaded quality factor of the resonator with a hypothetical sample, which has the dielectric permittivity of the real sample but has no loss ($\tan\delta=0$). This value is close to the unloaded Q_{00} of the split DR without the sample and can be found from the equation:

$$Q_{0\text{DR}}^{-1} = K_{1\parallel}\times\tan\delta_\parallel + K_{1\perp}\times\tan\delta_\perp, \tag{8}$$

where $K_{1\parallel}=W_{1\parallel}^E/W_\Sigma$, $K_{1\perp}=W_{1\perp}^E/W_\Sigma$ and $W_{1\parallel}^E+W_{1\perp}^E=W_1^E$. Here $W_{1\parallel}^E$ and $W_{1\perp}^E$ are the energies stored in the longitudinal and transverse components of the electric field $\vec{E}$ in the sapphire disks with the sample between them; $\tan\delta_\parallel$, $\tan\delta_\perp$ are the components of the loss tangent tensor of sapphire in the direction of the optical axis and in the plane perpendicular to this axis, respectively.

Similarly to Eqs. (6) and (7) the coefficients $K_{1\parallel}$ and $K_{1\perp}$ are calculated via integration of longitudinal and transverse components of vector $\vec{E}$ or by numerical differentiation of the resonance frequency dependences

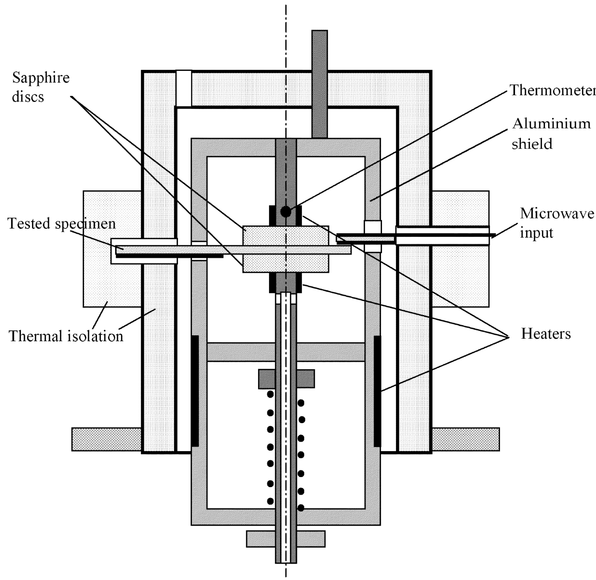

FIG. 3. Measurement cell draft.

$$K_{1\parallel} = -2\frac{\varepsilon_{1\parallel}}{\omega}\left(\frac{\partial\omega}{\partial\varepsilon_{1\parallel}}\right), \quad K_{1\perp} = -2\frac{\varepsilon_{1\perp}}{\omega}\left(\frac{\partial\omega}{\partial\varepsilon_{1\perp}}\right). \tag{9}$$

The inequalities $K_{1\parallel} \gg K_{1\perp}$ for HE_{n11} modes and $K_{1\parallel} \ll K_{1\perp}$ for EH_{n11} modes are typically valid.

C. Measurements of the surface resistance

To measure the surface resistance R_S of the metallic foil from the dielectric side, the disk 1 is cuddled to the unclad surface of the sample [Fig. 1(a) and Fig. 6(d) below]. In order to determine R_S we will use the values of the filling factor K_{3E} of the laminated sample and the unloaded quality factor $Q_{0\mathrm{DR}}$ of the resonator as well as tan δ of the unclad sample measured as it has been described in the previous section. Similar to Eq. (4) and taking Eq. (5) into account the unloaded quality factor $Q_{0\Sigma\sigma}$ of the resonator cuddled to the dielectric sample with metallization layer is defined as

$$\frac{1}{Q_{0\Sigma\sigma}} = \frac{P_{\Sigma\sigma}}{\omega W_\Sigma} = \frac{1}{Q_{0DR}} + K_{3E} \times \tan\,\delta + \frac{1}{Q_\sigma}, \tag{10}$$

where $P_{\Sigma\sigma}$ is the total loss power, $Q_\sigma = \omega W_\Sigma / P_\sigma$ is a partial Q factor due to ohmic loss in the metal foil, P_σ is an ohmic loss power, which equals to

$$P_\sigma = R_S \int_S |H_\tau|^2 dS/2, \tag{11}$$

where H_τ is the tangential component of the microwave magnetic field on the metallic foil at the interface with substrate surface S.

Total energy W_Σ stored in the resonator can be found through the integration of the magnetic field energy in partial resonator volumes

$$W_\Sigma = \sum_i W_i^H, \quad W_i^H = \frac{\mu_0\mu_i}{2}\int_{V_i} (|H_{i\perp}|^2 + |H_{iz}|^2) dV. \tag{12}$$

Neglecting the contribution of the longitudinal component of the magnetic field in Eq. (12), from Eqs. (10)–(12) we get the surface resistance

$$R_S = \pi f_n \mu_0 M / Q_\sigma, \tag{13}$$

where $Q_\sigma^{-1} = Q_{0\Sigma\sigma}^{-1} - Q_{0DR}^{-1} - K_{3E} \times \tan\,\delta$ and the geometric factor

$$M = \frac{4\sum_i W_i^H}{\mu_0 \int_S |H_{3\perp}|^2 dS} = \frac{2\sum_i \mu_i \int_{V_i} |H_{i\perp}|^2 dV}{\int_S |H_{3\perp}|^2 dS}$$

$$= \frac{2\sum_i \mu_i \int_S |H_\perp(r,\varphi)|^2 dS \int_l Z_{iE}^2(z) dz}{\int_S |H_\perp(r,\varphi)|^2 dS \cdot Z_{3E}^2(0)},$$

where integrands will be further defined in Appendix A. For nonmagnetic materials ($\mu_i = 1$) the factor M in Eq. (13) can be written as follows:

$$M = \left(\frac{\varepsilon_{1\perp}A_1}{\varepsilon_3}\right)^2 I_1 + \left(\frac{\varepsilon_2 A_2}{\varepsilon_3}\right)^2 I_2 + I_3 + \left(\frac{\varepsilon_2 A_4}{\varepsilon_3}\right)^2 I_4.$$

The expressions for A_i, I_i are also given in Appendix A.

III. EXPERIMENT

A. Measurement setup and cell description

A simplified draft of the measurement cell is shown in Fig. 3. A sample is placed between polished sapphire disks with diameter 12.51 mm and height 2.54 mm, which are arranged inside a thick-wall aluminum shield with inner diameter of 25 mm. The diameter of the shield was chosen to exclude any influence of the metal wall on either the resonant frequencies or the quality factors of the sapphire disks. The aluminum shield is placed inside a thermal isolation chamber. The lower sapphire disk is attached to the post guide and clamped to the sample through the spring with the pressure about three bars.

We took special care to prepare "nearly ideal" DR. Both DR disks were cut from the same piece of carefully oriented sapphire single crystal of very high chemical purity. The dimensions of both disks were identical to an accuracy of within 1 μm. The c-axis was perpendicular to disks faces. The faces of each disk were parallel with the accuracy better than 1 μm across the disk diameter. Surface roughness reduced to 2 nm after polishing. The deviation from flatness of each surface was less than 0.5 μm across disk diameter. As a result the problem of the residual air-gap was significantly reduced even when the two disks were brought into contact without a "soft" dielectric film between them. Moreover, because these two disks in close mechanical contact constitute a nearly perfect single crystal, no measurable splitting of the resonance curves has been detected.

To provide the process of dielectric samples replacement, the post guide is designed to be axially moveable and to have no radial free play. The aluminum shield with sapphire disks and test sample can be moved toward and away from the microwave excitation microstrip line by a steppermotor (not shown) in order to tune the coupling of the resonator and the excitation line. Semirigid coaxial cables connect the microstrip to standard 2.9 mm connectors outside

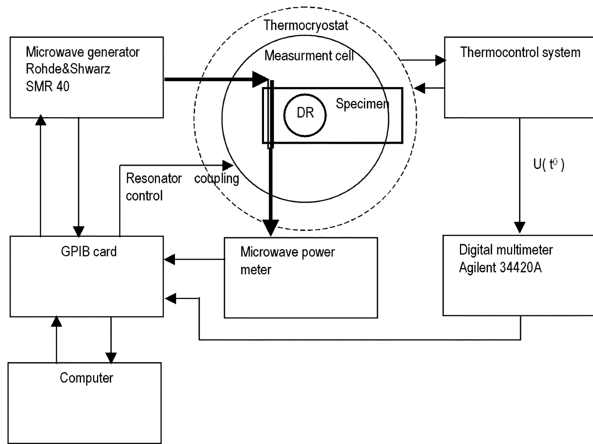

FIG. 4. The block-diagram of the measurement setup.

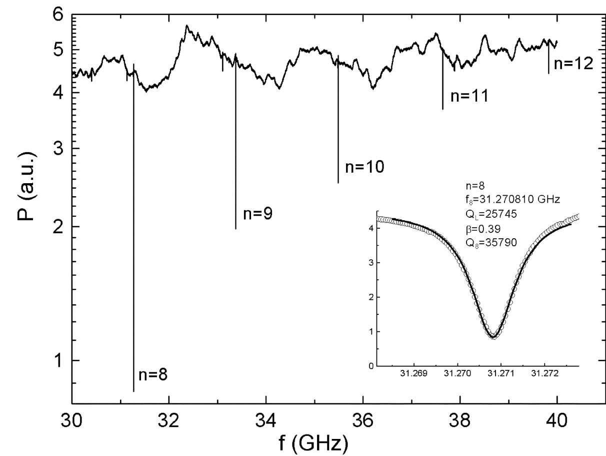

FIG. 5. Resonant spectrum of the single DR.

the thermal isolation. The measurement cell is placed in a stainless steel vacuum cryostat with a temperature control system. For low temperature measurements, liquid nitrogen needs to be evaporated from the cryostat and its vapor flows around the resonator and the aluminum shield. The block-diagram of the measurement setup is shown in Fig. 4.

We have paid special care on the absence of dust or fibers between the sapphire disks and/or sample to be measured. The value of the resonance frequency of the double resonator without a sample was used as a control parameter related to the sapphire face contamination. When necessary the faces of the split sapphire resonator were cleaned with special tissue prior to the measurements.

B. Further experimental procedure details and results

The procedure for taking the measurements of the dielectric constant, loss tangent, and surface resistance of one-side laminated dielectric samples is described below.

At first, the resonant spectrum (microwave power P versus frequency f) of the upper DR is measured. For this measurement the lower resonator is moved away by a maximum distance of 3 mm from the upper one and does not influence the measured quantities. Thereupon we determine the resonance frequencies f_n, loaded quality factors Q_n, and coupling coefficients β_n of HE_{n11} modes $(8 \leqslant n \leqslant 12)$ of the upper resonator in the range $30 \leqslant f_n \leqslant 40$ GHz. The coupling coefficient β_n is determined as

$$\beta_n = (1 - \sqrt{P_{0n}/P_{\infty n}}) \cdot (1 + \sqrt{P_{0n}/P_{\infty n}})^{-1},$$

where $P_{0n}, P_{\infty n}$ are the output power at the resonance frequency and nonresonance power level, respectively.

An example of the frequency spectrum measured at room temperature $T = 22\,^\circ\mathrm{C}$ for a single DR is shown in Fig. 5. The inset to Fig. 5 shows the experimental $P(f)$ curve corresponding to the HE_{811} mode (circles) and the results of the Lorentzian curve fit (solid line). An iterating method of least squares was used for fitting. An extensive description of this procedure will be published elsewhere. The unloaded quality factor $Q_8 = 35\,790$ for this mode was obtained by the standard formula $Q_8 = Q_L(1+\beta_8)$,[16] where Q_L is the measured (loaded) quality factor. The unloaded quality factors of the HE_{n11} modes with $n = 9,10,11,12$ are equal to 40 850, 45 360, 44 970, and 37 080, respectively. The maximum quality factor corresponds to $HE_{10,1,1}$ mode. The further increase of azimuth index n results in a drop in Q_n due to the increase of the sapphire loss tangent. The latter is roughly proportional to the frequency.

The measured values of the resonance frequencies and quality factors for HE_{n11} modes of the single resonator at different temperatures $-50 \leqslant T \leqslant 70\,^\circ\mathrm{C}$ are saved into computer memory as calibration constants for further calculations of the dielectric constant, loss tangent and surface resistance of laminated dielectric samples.

Next we proceed with similar measurements when both sapphire disks are clamped together and determine the values of resonant frequencies and quality factors for HE_{n11} modes of this doubled DR at the same temperatures $-50 \leqslant T \leqslant 70\,^\circ\mathrm{C}$. The results obtained are also stored in the computer memory.

The measured frequencies $f_n^{(2)}$ of the double DR are significantly lower than corresponding frequencies $f_n^{(1)}$ of the single one. The difference $(f_n^{(1)}\text{-}f_n^{(2)})$ decreases with the azimuth number n increase. For example, it equals 4406 MHz for $n = 9$ and 3637 MHz for $n = 12$. This approximately corresponds to the theoretical calculations for the double resonator. Results of theoretical calculations using Eqs. (1) and (2) are shown in Table I along with the measured resonance frequencies. Since high quality sapphire crystals demonstrate the same values of permittivity and do not show significant frequency dispersion, in these calculations we used our previous measurements of sapphire permittivities $\varepsilon_{1\parallel} = 11.577$ and $\varepsilon_{1\perp} = 9.388$.[17] From the quality factor of the resonator the loss tangent of our sapphire can be estimated at 2.5×10^{-5}. The relative discrepancy $\delta f = (f_{\mathrm{calc}} - f_n)/f_n$ between the calculated f_{calc} and measured f_n frequency values does not exceed 1.3% for the single DR and 0.5% for the double one. This discrepancy does not affect further results since the experimentally determined frequency shifts of the resonator with and without sample are used as the input for calculations.

The procedure for the measurements of the dielectric constant and loss tangent of an unclad thin dielectric sample has been described in parts A and B of Sec. II. Dielectric samples used for our measurements had planar dimensions 25×50 mm^2, thickness up to 1 mm and one-side metallized

TABLE I. Theoretical and experimental resonance frequencies of HE_{n11} modes.

	Single resonator			Double resonator		
n	$f_{\rm calc}$, GHz	$f_n^{(1)}$, GHz	$\delta f\times 10^2$	$f_{\rm calc}$, GHz	$f_n^{(2)}$, GHz	$\delta f\times 10^2$
9	32.9767	33.3873	−1.23	28.8439	28.9808	−0.47
10	35.1495	35.4969	−0.98	31.2617	31.3881	−0.40
11	37.3448	37.6594	−0.84	33.6768	33.7958	−0.35
12	39.5590	39.8415	−0.71	36.0889	36.2041	−0.32

square surface of 25×25 mm^2. The sample was clamped between the sapphire disks (Fig. 6(a)) providing the latter being in the center of the square 25×25 mm^2 surface.

When the sample is clamped inside the split DR, the resonance frequencies $f_{n\varepsilon}$ shift down compared to the frequencies f_n of the single DR. The problem of identification of the $HE_{n,1,1}$ mode arises. Fortunately, however, the coupling of the $HE_{n,1,1}$ modes are the highest, and the frequency difference $\Delta f = f_{n,\varepsilon} - f_{n\text{-}1,\varepsilon}$ between the nearest $HE_{n,1,1}$ and $HE_{n-1,1,1}$ modes is almost independent on $n\geqslant 9$ as shown in Fig. 7.

One more opportunity to identify modes is the use of an approximate (with uncertainty of 20%) value of ε, which can be found from low-frequency capacity measurements, from Eqs. (1) and (2) we calculate the approximate frequency $f_{n,\varepsilon}^{\rm appr}$ for a particular mode with an index n and perform the frequency sweep in the range $f_{n,\varepsilon}^{\rm appr}\pm 200$ MHz looking for the deepest resonance. This procedure is then successively repeated for higher $HE_{n,1,1}$ modes. Immediately after the measurement at a particular mode is finished, the resonance curve is fitted in order to obtain resonance frequency, loaded quality factor, coupling coefficient, and unloaded quality factor. If necessary, the coupling between the resonator and the microwave line is changed to obtain the optimal sensitivity. In such case the measurement with a new coupling is repeated. Using Eqs. (1)–(9) the values of the permittivity and loss tangent are calculated. If the mode identification was correct, the results of calculations for all the modes give very close values for both the permittivity and the loss tangent. Finally, the mean values of the permittivity and the loss tangent are calculated using results obtained for all modes. The results are weighted according to the uncertainty of the resonance curve fitting. Examples of such results obtained for a

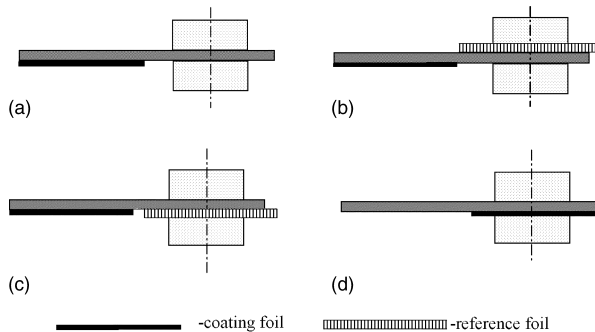

FIG. 6. Schemes for measurements of (a) ε, tan δ; (b) $R_{\rm Sref}$; (c) $Q_{\rm ref}$; (d) Q_σ, R_S.

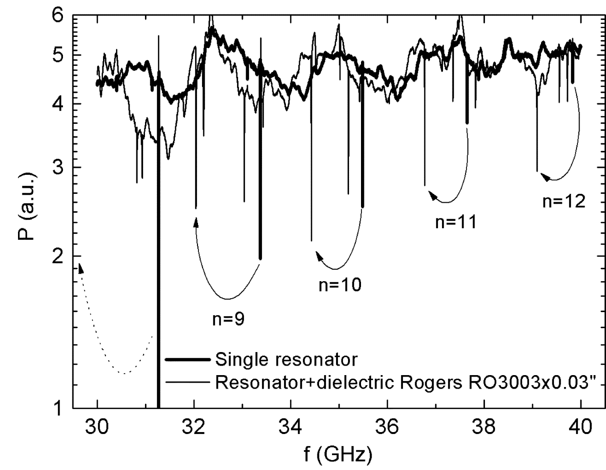

FIG. 7. Resonant spectra of a single DR and split DR with dielectric sample RO3003$\times$0.03″.

set of samples at room temperature are shown in Table II (Appendix B).

The test rig described above allows the measurements to be performed at different temperatures. Examples of the temperature dependences obtained for two samples, namely, NY9220$\times$0.01″ and Tly5a0200, are presented in Figs. 8 and 9 for the permittivity and loss tangent, respectively.

The method of surface resistance $R_{\rm S}$ measurements of the laminated dielectric samples is illustrated in Figs. 6(b)–6(d). Two approaches are possible here: (i) direct measurements and (ii) measurements using calibrated reference metal foil. Let us consider them separately.

(i) The direct method of the surface resistance measurements is based on the calculation of R_S using Eq. (13). In this case the sample is placed into the resonator as shown in Fig. 6(d) and the quality factor $Q_{0\Sigma\sigma}$ of the upper resonator with laminated dielectric sample is measured. Using the previously determined quality factor $Q_{\rm 0DR}$ of the resonator without a sample and the sample loss tangent tan δ (obtained by measuring the unclad part of the sample as described above) the value of Q_σ is obtained

$$Q_\sigma = (Q_{0\Sigma\sigma}^{-1} - Q_{0DR}^{-1} - K_{3E}\times \tan\,\delta)^{-1}, \tag{14}$$

where filling factor K_{3E} is calculated for laminated sample. Factor Q_σ has already appeared before as a denominator in the right side of Eq. (13). It characterizes an ohmic loss in the metal lamination at the interface with dielectric material. The geometric factor M is calculated from Eq. (13).

The accuracy of the direct surface resistance measurements depends strongly on the thickness t and the dielectric losses in the substrate. To obtain reliable results by this method, the ohmic losses in the laminated metal should be greater than or comparable with the dielectric losses. Figure 10 illustrates the frequency shifts and the quality factor variations for direct R_S measurements at $HE_{10,1,1}$ mode.

In case of copper foil the applicability criteria for direct measurements can be written as

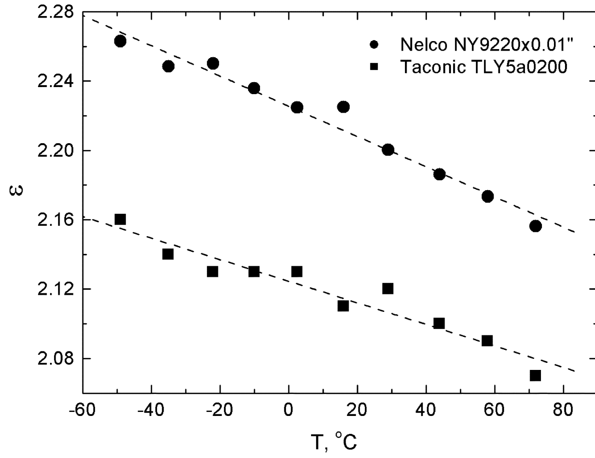

FIG. 8. Temperature dependences of the permittivity of NY9220×0.01″ (Nelco) and Tly5a0200 (Taconic).

$t < 0.1(\varepsilon/\tan\,\delta)$, where the thickness t of the substrate is expressed in μm. In Table II the R_S data of RO3003×0.01", GIG M/L-2, NH9348ST0203CHCH, Rogers 3003, Rogers 5880, Sheldahl G2200×2mil, and Sheldahl Comclad XF ×10mil samples were obtained by direct measurements.

(ii) The second method to measure the surface resistance of laminated dielectric samples involves a few extra steps, which are shown in Figs. 6(b)–6(d). These steps are described in more detail below:

(1) A smooth copper foil is chosen as the reference one. The surface resistance of the foil $R_{\mathrm{Sref}}(f)$ is determined by measuring the quality factor of the upper DR pressed to this foil [Fig. 6(b)]. Using the measurements of f_n, $Q_{0\Sigma\sigma}$ for $HE_{n,1,1}$ modes the surface resistance can be calculated as $R_{\mathrm{Sref}} = \pi f_n \mu_0 M_{\mathrm{ref}}/Q_{\sigma\mathrm{ref}}$, where $Q_{\sigma\mathrm{ref}}^{-1} = Q_{0\Sigma\sigma}^{-1} - Q_{\mathrm{ODR}}^{-1}$, $M_{\mathrm{ref}} = (\varepsilon_{1\perp}A_1/\varepsilon_2)^2 I_1 + I_2 + A_4^2 I_4$. The expression for M_{ref} follows from Eq. (13) for the resonator located on a metallic plane without dielectric layer ($t=0$) but with the effective air-gap d. In its turn, the effective air-gap d can be found from Eqs. (1) and (2) and the condition of equality of the resonance frequency of double resonator with $2d$ air-gap to the frequency of the upper DR on the metal surface. To find A_i and I_i values from Eqs. (A6) of Appendix A, one should use $t=0$ and obtained air-gap value d.

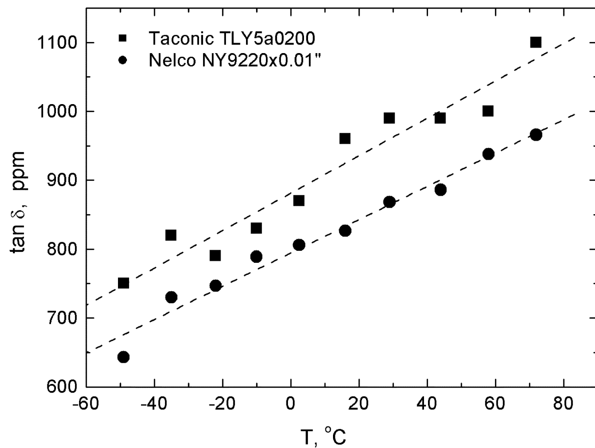

FIG. 9. Temperature dependences of the loss tangent of NY9220×0.01″ (Nelco) and Tly5a0200 (Taconic).

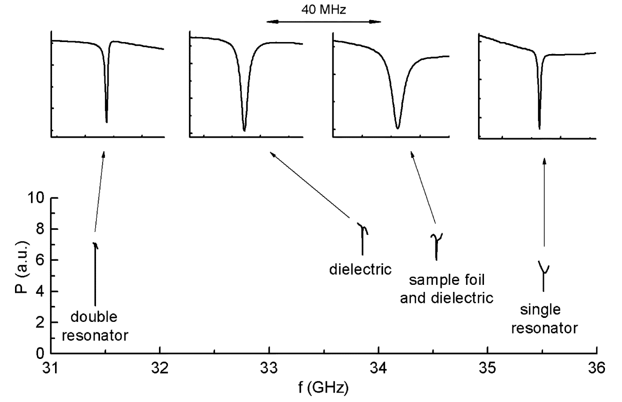

FIG. 10. The evolution of resonance curves when measuring the surface resistance of RO3003×0.03″ sample.

(2) The reference foil is placed underneath the unclad region of the dielectric sample, and they are clamped together between the sapphire disks [Fig. 6(c)]. The quality factors $Q_{0\Sigma\sigma\mathrm{ref}}$ of this sandwich structure are measured for different resonance $HE_{n,1,1}$ modes. The values of Q_{ref} at the resonance frequencies are to be found by the formula

$$Q_{\mathrm{ref}} = (Q_{0\Sigma\mathrm{ref}}^{-1} - Q_{0\mathrm{DR}}^{-1} - K_{3\mathrm{E}} \times \tan\,\delta)^{-1} \quad (15)$$

In contrast to $Q_{\sigma\mathrm{ref}}$ determined at the first step [Fig. 6(b)], the quality factor Q_{ref} in Eq. (15) determines the loss in the reference foil under dielectric substrate [Fig. 6(c)].

(3) The quality factor Q_σ related to the ohmic loss at the interface between the laminated metal foil and the dielectric material [Fig. 6(d)] is to be determined in accordance with Eq. (14). The surface resistance R_S of the metal foil at the resonance frequency of $HE_{n,1,1}$ mode can be found as follows: $R_S = R_{\mathrm{Sref}} Q_{\mathrm{ref}}/Q_\sigma$, where the value of R_{Sref} measured at the first step is linearly approximated to the appropriate frequency of the third measurement step.

Method (ii) has the evident advantage when comparing it to the direct one (i), namely, the surface resistance R_S does not depend on the calculation of the geometric factor M in Eq. (13) and, hence, the accuracy of method (ii) is higher, especially for thicker samples.

IV. DISCUSSION

The presented technique allows the measurements of the dielectric constant (from 2 to 10) and loss tangent (from 10^{-4} to 10^{-2}) of dielectric substrates with reasonable accuracy for substrate thickness ranging from 50 to 1000 μm. Measurements of well-known samples and reproducibility of the results on different modes (see Table II) show the accuracy of about 1% in permittivity and 10% in loss tangent. For precise measurements of samples with $\varepsilon > 5$, however, thinner samples ($d < 300$ μm) are more preferable. A resonance

technique providing the electric field orthogonal to the surface of the substrate has been demonstrated. The high sensitivity became possible owing to high unloaded quality factor of the sapphire "whispering gallery" resonator and substantial filling factor value even when very thin substrates are to be measured. The main source of the inaccuracy of the measurements of thin dielectric films using our method arises from the uncertainty in the samples thickness. There is no fundamental restriction on the maximum thickness of the substrate while its dielectric permittivity is lower than the one of sapphire. When the substrate thickness increases, the measurement structure shown in Fig. 1 gradually turns to single DR on the dielectric half-space. In such a case, a single DR resonance spectrum represented in Fig. 4 just shifts to lower frequencies. The contribution of the second substrate face consequently vanishes due to the exponential decay of the electromagnetic field in the substrate thickness.

The temperature range from $-50°$ to $+70°$C shown for our setup can be easily extended down to liquid nitrogen temperature and up to samples melting or plastic deformation temperature providing stronger thermal isolation of the setup and the usage of thermostable plastic parts of the construction.

Experimental results do not show any influence of the residual air-gap problem, which is explained by the optical-quality sapphire polishing, elasticity or/and flatness of most of the samples, as well as by pressure applied between sapphire disks and the substrate. Nevertheless, the measurement setup was found to be sensitive to contamination of the surface of the test samples. This peculiarity is inherently caused by the orthogonality of the electric field to the surface of the sample. Thus, one has to pay special care to the absence of dust or fibers between the surfaces of the substrate and/or the sapphire disks.

The method described also provides reasonable accuracy of the surface resistance measurements of the metal lamination. The presence of metal film in the resonator reduces the quality factor by an order of magnitude. The inaccuracy in the surface resistance of the metal lamination at the interface with dielectric layer is strongly influenced by the substrate thickness, dielectric constant, and loss tangent. In the case of $\varepsilon \geqslant 2$ and $\tan\,\delta \sim 10^{-4}$ the accuracy of 15–20% in R_S measurements was shown experimentally for dielectric substrate thickness $t \leqslant 0.2 \div 0.5$ mm. Such materials are widely used in 30–40 GHz frequency range. The accuracy of the direct surface resistance measurements strongly depends on the thickness t and the dielectric losses in the substrate. To obtain reliable results by this method the ohmic losses in the laminated metal should be greater or comparable to dielectric losses. In case of copper foil the applicability criteria for direct measurements can be written as $t < 0.1(\varepsilon/\tan\,\delta)$, where the thickness t of the substrate is expressed in microns. Measurements of polished copper R_S showed the values which are very close to the minimal theoretical value of about $0.05\ \Omega$ at our frequencies. However, most of the samples shown in Table II demonstrated several times higher surface resistance values. This fact can be accounted by the surface roughness and the presence of adhesive layers such as zinc. Poor quality of the laminating surfaces adjacent to the dielectric was actually seen on the detached foils through the microscope.

ACKNOWLEDGMENTS

We would like to thank V. Zhitomirsky and M. McLean for stimulating discussions. The technical help of S.V. Ryzhkov, V.N. Kurlov, and G.E. Tsydynzhapov is gratefully aknowledged. The work was supported by the National Measurement System Directorate of the U.K. Department of Trade and Industry. Yu. A. Nefyodov thanks Russian Science Support Foundation.

APPENDIX A: ELECTROMAGNETIC FIELD IN THE RESONATOR

We represent an electromagnetic field inside the resonator [Fig. 1(a)] within the boundaries $t+d \leqslant z \leqslant t+d+L$ as a hybrid standing HE or EH wave along the z-axis. The transverse field distribution in the gap 2, dielectric layer 3, and top space 4 in Fig. 1(b) is assumed the same as in the disk 1. A set of Maxwell equations result in a corresponding set of wave equations for longitudinal field components inside the dielectric cylinder $r \leqslant a$ (the space marked as (+) in Fig. 1)[13]

$$\nabla^2\Psi^+_{iE} + k_i^2(\varepsilon_{1\parallel}/\varepsilon_{1\perp})\Psi^+_{iE} - \left(1 - \frac{\varepsilon_{1\parallel}}{\varepsilon_{1\perp}}\right)\frac{\partial^2\Psi^+_{iE}}{\partial z^2} = 0,$$
$$\nabla^2\Psi^+_{iH} + k_i^2\Psi^+_{iH} = 0, \tag{A1}$$

where $\Psi^+_{iE}=E^+_{iz}(r,\varphi,z)$, $\Psi^+_{iH}=H^+_{iz}(r,\varphi,z)$ and $i=1,2,3,4$ are the numbers for dielectric layers along the z-axis. In the space outside the dielectric cylinder, $r>a$, marked as (−) in Fig. 1, the longitudinal field components should satisfy the following condition:

$$\nabla^2\Psi^-_{iE,H} + k_2^2\Psi^-_{iE,H} = 0, \tag{A2}$$

where $\Psi^-_{iE}=E^-_{iz}(r,\varphi,z)$, $\Psi^-_{iH}=H^-_{iz}(r,\varphi,z)$ and $i=1,2,3,4$.

We look for the solutions of Eqs. (1) and (2) in the form of

$$E^\pm_{iz} = R^\pm_E(r)\Phi_E(\varphi)Z_{iE}(z), \quad H^\pm_{iz} = jR^\pm_H(r)\Phi_H(\varphi)Z_{iH}(z),$$
$$i = 1,2,3,4, \tag{A3}$$

where

$$R^+_E(r) = A^+J_n(\alpha\chi_1 r), \quad R^-_E(r) = A^+\frac{J_n(\alpha\chi_1 a)}{H_n^{(2)}(\chi_2 a)}H_n^{(2)}(\chi_2 r),$$

$$\Phi_E(\varphi) = \begin{pmatrix}\cos n\varphi\\ \sin n\varphi\end{pmatrix},$$

$$R^+_H(r) = B^+J_n(\chi_1 r), \quad R^-_H(r) = B^+\frac{J_n(\chi_1 a)}{H_n^{(2)}(\chi_2 a)}H_n^{(2)}(\chi_2 r),$$

$$\Phi_H(\varphi) = \begin{pmatrix}-\sin n\varphi\\ \cos n\varphi\end{pmatrix},$$

A^+, B^+ are the constants, χ_1 and χ_2 are the inner $(0 \leqslant r \leqslant a)$ and the outer $(a \leqslant r < \infty)$ transverse wave numbers, respectively, $\alpha = \sqrt{\varepsilon_{1\parallel}/\varepsilon_{1\perp}}$. As $Z_{iE,H}(z)$ functions we choose the ones

$$Z_{iE}(z)=\left\{\begin{array}{l}A_1\cos(hz+\Theta_1)\\ A_i\cosh(h_{iE}z+\Theta_i)\\ A_4\exp(-h_{4E}z)\end{array}\right\},\quad \begin{array}{l}(t+d\leqslant z\leqslant t+d+L)\\ i=2,3;\quad (0\leqslant z\leqslant t; t\leqslant z\leqslant t+d)\\ (t+d+L\leqslant z<\infty)\end{array}$$

$$Z_{1H}(z)=-A_1\sin(hz+\Theta_1),\quad (t+d\leqslant z\leqslant t+d+L), \tag{A4}$$

Neglecting the components H_{iz} and their contribution to transverse components of HE_{n11} modes within gap 2 and layers 3,4

$$Z_{iH}(z)=0,\quad i=2,3,4;\quad (0\leqslant z\leqslant t;\quad t\leqslant z<t+d;\quad t+d+L<z<\infty).$$

Here A_i are the constants and h_{iE} are the longitudinal wave numbers ($h_{4E}=h_{2E}$).

The transverse field components in the resonator are related to the longitudinal ones through well-known formulas[16] and can be expressed as follows:

$$E_{1r}^{\pm}=\frac{-A_1}{(\chi^{\pm})^2}\left[h\frac{\partial}{\partial r}R_E^{\pm}(r)\Phi_E(\varphi)+\frac{\omega\mu_0\mu_1}{r}R_H^{\pm}(r)\frac{\partial}{\partial\varphi}\Phi_H(\varphi)\right]\times\sin(hz+\Theta_1),$$

$$E_{1\varphi}^{\pm}=\frac{-A_1}{(\chi^{\pm})^2}\left[\frac{h}{r}R_E^{\pm}(r)\frac{\partial}{\partial\varphi}\Phi_E(\varphi)-\omega\mu_0\mu_1\frac{\partial}{\partial r}R_H^{\pm}(r)\Phi_H(\varphi)\right]\times\sin(hz+\Theta_1),$$

$$E_{ir}^{\pm}=\frac{-A_i}{(\chi^{\pm})^2}h_{iE}\frac{\partial}{\partial r}R_E^{\pm}(r)\Phi_E(\varphi)\sinh(h_{iE}z+\Theta_i),$$

$$E_{i\varphi}^{\pm}=\frac{-A_i}{(\chi^{\pm})^2}\frac{h_{iE}}{r}R_E^{\pm}(r)\frac{\partial}{\partial\varphi}\Phi_E(\varphi)\sinh(h_{iE}z+\Theta_i),\quad i=2,3,$$

$$E_{4r}^{\pm}=\frac{-A_4}{(\chi^{\pm})^2}h_{2E}\frac{\partial}{\partial r}R_E^{\pm}(r)\Phi_E(\varphi)\exp(-h_{2E}z),$$

$$E_{4\varphi}^{\pm}=\frac{-A_i}{(\chi^{\pm})^2}\frac{h_{2E}}{r}R_E^{\pm}(r)\frac{\partial}{\partial\varphi}\Phi_E(\varphi)\exp(-h_{2E}z),$$

$$H_{1r}^{\pm}=j\frac{A_1}{(\chi^{\pm})^2}\left[\frac{\omega\varepsilon_0\varepsilon_{1\perp}}{r}R_E^{\pm}(r)\frac{\partial}{\partial\varphi}\Phi_E(\varphi)-h\frac{\partial}{\partial r}R_H^{\pm}(r)\Phi_H(\varphi)\right]\times\cos(hz+\Theta_1),$$

$$H_{1\varphi}^{\pm}=-j\frac{A_1}{(\chi^{\pm})^2}\left[\omega\varepsilon_0\varepsilon_{1\perp}\frac{\partial}{\partial r}R_E^{\pm}(r)\Phi_E(\varphi)+\frac{h}{r}R_H^{\pm}(r)\frac{\partial}{\partial\varphi}\Phi_H(\varphi)\right]\times\cos(hz+\Theta_1),$$

$$H_{ir}^{\pm}=j\frac{A_i}{(\chi^{\pm})^2}\frac{\omega\varepsilon_0\varepsilon_i}{r}R_E^{\pm}(r)\frac{\partial}{\partial\varphi}\Phi_E(\varphi)\cosh(h_{iE}z+\Theta_i),$$

$$H_{i\varphi}^{\pm}=-j\frac{A_i}{(\chi^{\pm})^2}\omega\varepsilon_0\varepsilon_i\frac{\partial}{\partial r}R_E^{\pm}(r)\Phi_E(\varphi)\cosh(h_{iE}z+\Theta_i),\quad i=2,3,$$

$$H_{4r}^{\pm}=j\frac{A_4}{(\chi^{\pm})^2}\frac{\omega\varepsilon_0\varepsilon_2}{r}R_E^{\pm}(r)\frac{\partial}{\partial\varphi}\Phi_E(\varphi)\exp(-h_{2E}z),$$

$$H_{4\varphi}^{\pm}=-j\frac{A_4}{(\chi^{\pm})^2}\omega\varepsilon_0\varepsilon_2\frac{\partial}{\partial r}R_E^{\pm}(r)\Phi_E(\varphi)\exp(-h_{2E}z), \tag{A5}$$

where $\chi^+=\chi_1$, $\chi^-=\chi_2$.

The boundary conditions $E_{1\varphi}^+=E_{1\varphi}^-, H_{1\varphi}^+=H_{1\varphi}^-$ for inside (+) and outside (−) field components at $r=a$ within the limits $t+d\leqslant z\leqslant t+d+L$ ($i=1$) will result in Eq. (1). Assuming the constant A_3 being equal to unity and neglecting the contributions of H_{1z} in the expressions for $E_{1r},E_{1\varphi},H_{1r},H_{1\varphi}$ to satisfy the boundary conditions at $z=0$, $z=t$, $z=t+d$, $z=t+d+L$, we get Eq. (2) and the following relations:

$$A_1=A_2\cdot\frac{\cosh[h_{2E}(t+d)+\Theta_2]}{\varepsilon_\perp\cos[h(t+d)+\Theta_1]},\quad A_2=\frac{\varepsilon_3\cosh(h_{3E}t)}{\varepsilon_2\cosh(h_{2E}t+\Theta_2)},$$

$$A_4=A_1\frac{\varepsilon_\perp\cos[h(t+d+L)+\Theta_1]}{\exp[-h_{2E}(t+d+L)]},$$

$$\Theta_1=-\arctan\left[\frac{\varepsilon_\perp h_{2E}}{h}\tanh[h_{2E}(t+d)+\Theta_2]\right]-h(t+d),$$

$$\Theta_2=\operatorname{arctanh}\left[\frac{\varepsilon_2h_{3E}}{\varepsilon_3h_{2E}}\tanh(h_{3E}t)\right]-h_2t,\quad \Theta_3=0$$

$$I_1=L+\frac{\sin\{2[h(t+d+L)+\Theta_1]\}-\sin\{2[h(t+d)+\Theta_1]\}}{2h},$$

$$I_2=d+\frac{\sinh\{2[h_{2E}(t+d)+\Theta_2]\}-\sinh[2(h_{2E}t+\Theta_2)]}{2h_{2E}},$$

$$I_3=t+\frac{\sinh(2h_{3E}t)}{2h_{3E}},\quad I_4=\frac{\exp[-2h_{2E}(t+d+L)]}{2h_{2E}}. \tag{A6}$$

APPENDIX B: SAMPLES PARAMETERS AT ROOM TEMPERATURE

In Table II below the average values of the permittivity and loss tangent, the coefficients $C_\varepsilon=[\partial\varepsilon/(\varepsilon\times\partial t)]1000$ and $C_\delta=[\partial(\tan\delta)/(\tan\delta\times\partial t)]1000$ are shown. These values are introduced as correction coefficients describing the influence of the absolute uncertainty Δt (in microns) in measurements of the thickness of the sample. The error for permittivity can then be found by the formula $\Delta\varepsilon/\varepsilon=C_\varepsilon\times\Delta t/1000$. Similarly, the error in the loss tangent value is given by $\Delta(\tan\delta)/\tan\delta=C_\delta\times\Delta t/1000$.

TABLE II. Samples parameters.

Samples																	
Manufacturers Info			Average values						Values for particular mode (9–12)								
Sample/Company material ε/tan $\delta\times10^3$ @10GHz	Thickness, μm	ε flow frequency	ε C_ε	$\pm\Delta\varepsilon$	tan $\delta\times10^3$ C_δ	$\pm\Delta$ tan $\delta\times10^3$	R_{sr} ohm	$\pm\Delta R_s$ Ohm	$f_{\rm diel}$ GHz	$Q_{\rm diel}$	Uncertainty, %	ε	tan $\delta\times10^3$	$f_{\rm metal+diel,}$ GHz	$Q_{\rm metal+dial}$	Uncertainty, %	$R_{\rm si}$Ohm
RO3003×0.01”/Rogers	255	2.92	2.85	0.03	1.3	0.1	0.24	0.14	31.045	9020	4.8	2.80	0.77	31.733	2806	5.4	0.38
PTFE ceramic									33.499	6833	4.0	2.84	1.28	34.159	4584	2.9	0.24
3.0/1.3			2.43		−1.0				35.949	7812	1.2	2.85	1.27	36.551	5986	5.8	0.22
									38.375	8565	8.3	2.85	1.28	38.916	6694	14.1	0.28
RO3003×0.02″/Rogers	505	2.90	2.96	0.02	1.4	0.2	0.17	0.02	31.670	6183	2.9	2.97	1.28	36.970	5345	2.9	0.17
PTFE ceramic									34.099	6871	0.4	2.96	1.42	39.264	6787	15.8	0.18
3.0/1.3			1.11		−0.49				36.490	7526	1.3	2.96	1.56				
									38.854	9462	3.8	2.96	1.38				
RO3003×0.03″/Rogers	760	2.94	2.93	0.02	1.7	0.3	0.09	+0.1	32.035	4401	13.8	2.97	2.16	32.513	3242	5.4	0.18
PTEF ceramic								−0.04	34.418	6394	4.5	2.93	1.84	34.800	4219	6.1	0.10
3.0/1.3			0.640		−0.055				36.759	8054	4.1	2.93	1.76	37.075	5755	0.6	0.06
									39.080	10241	1.0	2.94	1.50	39.344	9229	5.3	0.10
NY9220×0.03″/Nelco	755	2.23	2.09	0.02	0.98	0.14	0.110	0.016	32.478	11512	0.7	2.09	0.98	32.833	7720	10.9	0.12
Woven PTFE									34.768	13334	7.7	2.09	1.08	35.067	11570	1.4	0.11
2.2/1.3			0.707		−0.16				37.053	16623	3.2	2.09	1.01	37.297	14484	7.1	0.10
									39.327	18145	3.7	2.09	0.84	39.531	16103	1.7	0.11
NY9220×0.01”/Nelco	245	2.25	2.21	0.02	0.86	0.26	0.25	0.03	31.400	10585	5.4	2.22	0.69	32.149	6064	8.1	0.230
Woven PTFE									33.854	10733	0.8	2.21	0.83	34.519	7902	1.3	0.244
2.2/1.3			2.97		−0.87				36.274	10290	2.0	2.20	1.06	36.860	9863	5.5	0.256
									38.667	12360	2.7	2.21	0.95	39.181	11470	1.8	0.259
GIG M/L−2/isola	75	3.85	2.90	0.02	7.8	0.7			29.835	1798	1.5	2.89	7.91				
									32.314	1829	2.5	2.90	8.10				
			9.74		−3.8				34.784	2060	1.7	2.90	7.51				
									37.243	1956	5.2	2.92	8.32				
NH9348ST0203CHCH/	205	3.60	3.32	0.03	3.1	1.2	0.36	0.1	30.512	2924	2.7	3.32	2.95	31.191	1308	2.3	0.25
Neltec									35.499	3270	0.8	3.30	3.27	33.929	1390	11.8	0.15
PTFE/glass/ceramic			2.94		−1.6				37.949	601	11.1	3.33	21.3	36.111	2566	4.1	0.46
3.48/3																	
NY9208ST0762CHCH/	800	2.20	1.96	0.02	0.49	0.15	0.12	0.06	32.573	18 632	2.5	1.96	0.49	32.898	12081	6.2	0.12
Neltec									34.846	20 234	10.3	1.96	0.57	35.121	16826	3.0	0.11
PTFE woven			0.585		−0.11				37.117	23 638	10.4	1.95	0.52	37.341	21609	3.7	0.17
2.08/0.6									39.379	25 726	4.7	1.96	0.41	39.568	23930	5.7	0.11
fly 5a0200/Taconic	525	1.80	2.12	0.02	0.94	0.05	0.09	0.04	32.219	10 355	3.5	2.11	0.93	32.700	6228	2.5	0.06
PTFE/glass									34.546	12 691	2.1	2.13	0.93	34.966	9766	0.7	0.11
2.17/0.4			1.22		−0.32				36.872	14 400	2.1	2.13	0.97	37.221	13156	4.7	0.08
									39.181	16 618	2.0	2.13	0.92	39.474	13793	2.5	0.09
teflon395	395	2.00	2.03	0.03	0.19	0.05			32.005	22 823	3.6	2.06	0.20				
									34.403	27 812	1.0	2.01	0.18				
			1.76		−0.47				36.755	28 090	0.7	2.00	0.20				
									39.086	30 672	1.5	1.99	0.15				
Cu-coated quartz 2	1000	3.80	3.88	0.03	0.63	0.07			31.791	10 118	100	3.87	0.60				
									34.201	12 896	100	3.86	0.57				
			0.362		−0.18				36.572	14 161	99.4	3.87	0.61				
									38.916	14 772	9.8	3.90	0.66				
Rogers 6002	395	2.94	2.83	0.02	1.2	0.1	0.13	+0.15	31.502	6507	1.7	2.84	1.19	34.546	6415	10.5	0.06
								−0.08	33.949	7768	1.1	2.82	1.19	36.877	7488	8.9	0.12
2.94/1.2			1.56		−0.67				36.360	8765	1.0	2.82	1.24	39.190	7800	5.1	0.21
									38.742	10371	5.2	2.83	1.15				
Rogers 3003	245	3.15	2.89	0.03	1.2	0.2	0.23	0.04	30.925	6768	1.9	2.93	1.10	31.682	3617	8.4	0.22
PTFE ceramic									33.433	8093	3.4	2.89	1.04	34.116	4997	6.1	0.19
3.1/1.3			2.51		−1.1				35.885	8001	1.7	2.89	1.21	36.513	6197	6.1	0.20
									38.315	8283	4.4	2.90	1.31	38.8/82	6988	0.9	0.24
Rogers 5880	120	2.34	2.16	0.02	0.74	0.25	0.21	0.06	30.632	11 703	2.8	2.17	0.63	31.389	4114	3.9	0.175
PTFE/glass/fiber									33.115	12756	1.5	2.18	0.65	33.848	4579	5.7	0.219
2.2/0.9			6.14		−1.8				35.608	10 266	4.4	2.14	0.98	36.274	6067	1.4	0.197
									38.049	13 209	4.3	2.16	0.73	38.673	6463	3.5	0.242
Sheldahl G2200×2mil	50	1.4	2.99	0.02	12.9	0.9	0.13	0.02	29.561	1442	1.2	2.98	13.1	30.050	922	3.3	0.01
									32.024	1513	4.4	2.98	12.7	32.538	698	1.8	0.14
			13.3		−5.8				34.481	1547	1.1	2.99	12.8	35.016	932	1	0.12
									36.933	1590	4.5	3.01	12.8	37.479	534	46.4	0.12

TABLE II. (*Continued.*)

Samples									Samples parameters								
Manufacturers Info				Average values								Values for particular mode (9–12)					
Sheldahl Comclad	280	2.27	2.24	0.02	0.44	0.12	0.07	+0.05	31.518	20 103	5.1	2.26	0.24	32.243	10 044	4.3	0.10
XF × 10mil								−0.02	33.962	15 775	25.6	2.24	0.49	34.598	17 829	2.9	0.07
			2.48		−0.77				36.370	16 270	22.0	2.24	0.55	36.924	20 839	3.3	0.05
									38.753	18 707	29.1	2.24	0.47	39.235	22 934	3.0	0.5
tlc32-031	805	2.70	2.92	0.03	5.3	0.5	0.21		32.102	1116	2.1	2.92	9.84	37.073	3511	4.6	0.39
									34.455	2641	3	2.93	5.15	39.348	3850	0.5	0.03
			0.576		−0.21				36.799	3202	6.1	2.90	5.38				
									39.12	4015	3.2	2.89	5.24				
rdx1100060	155	3.72	3.07	0.03	4.2	0.3	0.13		30.365	2208	2.3	3.07	4.32	35.977	2054	2.5	0.13
									32.857	2508	3.6	3.08	4.14				
			3.92		−1.9				35.425	5531	0.8	2.91	1.92				
									37 816	2998	3.8	3.05	4.12				

[1] J. Baker-Jarvis, B. Riddle, and M. D. Janezic, *Dielectric and Magnetic Properties of Printed Wiring Boards and Other Substrate Materials* (NIST Technical Note 1512, 1999), p. 80; J. Baker-Jarvis, M. D. Janezic, B. Riddle, C. L. Holloway, N. G. Paulter, and J. E. Blendell, *Dielectric and Conductor-Loss Characterisation and Measurements of Electronic Packaging Materials* (NIST Technical Note 1520, 2001), p. 152.
[2] A. L. Cullen and P. K. Yu, Proc. R. Soc. London, Ser. A **325**, 493 (1971).
[3] R. J. Cook and R. J. Jones, IEEE Trans. Instrum. Meas. **IM-23**, 438 (1974).
[4] M. N. Afsar and K. J. Button, Proc. IEEE **73**, 131 (1985).
[5] L. A. Weinshtein, *Open Resonators and Open Waveguides* (Sovetskoe Radio, Moscow, 1966).
[6] H. E. Bussey, IRE Trans. Instrum. **9**, 171 (1960).
[7] A. Hernandes, E. Martin, and J. M. Zamarro, J. Phys. E **19**, 222 (1986).
[8] G. Kent, IEEE Trans. Instrum. Meas. **45**, 102 (1996).
[9] M. R. Trunin, J. Supercond. **11**, 381 (1998); Z. Zhai, C. Kusko, N. Hakim, and S. Sridhar, Rev. Sci. Instrum. **71**, 3151 (2000).
[10] T. Nishikawa, K. Wakino, H. Tanaka, and Y. Ishikawa, *CPEM' 88 Digest, Conference Precise Electromagnetic Measurements*, Tukuba (1988), p. 155.
[11] V. F. Vzjatyshev, V. S. Dobromyslov, V. L. Masalov, S. S. Nesterenko, and A. A. Potapov, Trudy Moskovskogo Energeticheskogo Instituta **360**, 51 (1978).
[12] V. N. Egorov, E. N. Panchenko, I. N. Zakharova, and E. Yu. Tokareva, Izv. Acad. Nauk Belorusskoj SSR, serija Fiziko-technicheskih nauk **4**, 66 (1989).
[13] V. N. Egorov and I. N. Mal'tseva, Electronnaja technika. Serija 1, Electronica SVCH **1**, 3 (1984).
[14] V. N. Egorov and I. N. Mal'tseva, Electronnaja technika. Serija 1, Electronica SVCH **2**, 36 (1984).
[15] V. F. Vzjatyshev and V. S. Dobromyslov, Trudy Moskovskogo Energeticheskogo Instituta **397**, 5 (1979).
[16] V. V. Nikol'skii and T. I. Nikol'skaja, *Electrodinamics and Radio-wave Propagation* (Nauka, Moscow, 1989).
[17] V. N. Egorov and A. S. Volovikov, Radiophys. Quantum Electron. **44**, 885 (2001).